Article

The Different Roles of Water in Photocatalytic DeNOx Mechanisms on TiO2: A Basis for Engineering Nitrate Selectivity?

Lu Yang, Amer Hakki, Fazhou Wang, and Donald E. Macphee

ACS Appl. Mater. Interfaces, **Just Accepted Manuscript** • Publication Date (Web): 05 May 2017

The Different Roles of Water in Photocatalytic DeNOx Mechanisms on TiO_2: A Basis for Engineering Nitrate Selectivity?

Lu Yang[†,‡] , Amer Hakki[†], Fazhou Wang[*‡] and Donald E Macphee[*†]

† Department of Chemistry, University of Aberdeen, Meston Building, Meston Walk, AB24 3UE, Aberdeen, Scotland, United Kingdom

‡ State Key Laboratory of Silicate Materials for Architectures, Wuhan University of Technology, 122# Luoshi Road, Wuhan 430070, China

Abstract: The nitrate selectivity of TiO_2 has important consequences for its efficiency as a NOx depollution photocatalyst. Most emphasis is typically given to photocatalyst activity, a measure of the rate at which NOx concentrations are reduced, but a reduction in NOx concentration (mainly NO + NO_2) is not necessarily a reduction in atmospheric NO_2 concentration because the catalytic process itself generates NO_2. With NO_2 being considerably more toxic than NO, more emphasis on nitrate selectivity, a measure of the NOx conversion to nitrate, and how to maximise it, should be given in engineering photocatalytic systems for improved urban air quality. This study, on the importance of adsorbed water in the photocatalytic oxidation of NOx, has identified important correlations which differentiate the role that water plays in the oxidation of NO and NO_2. This observation is significant and offers insights into controlling nitrate selectivity on TiO_2 and the potential for increased effectiveness in environmental photocatalyst applications.

Keywords: Supported TiO_2; Synthesis conditions; adsorbed water; NOx; Nitrate selectivity

* Corresponding Author: d.e.macphee@abdn.ac.uk (Donald E Macphee); fzhwang@whut.edu.cn (Fazhou Wang).

1. Introduction

Anthropogenic NOx gases (mainly NO and NO_2) are introduced to the atmosphere as a result of high temperature combustion processes. NOx gases are not only toxic in their own right but they contribute to the formation of other toxic atmospheric pollutants, such as ground level ozone, PAN (peroxyacytyl nitrate), etc. [1-3]. Consequently, EU and EPA guidelines for maximum atmospheric NO and NO_2 concentrations have been set but these are regularly exceeded in urban centers because the largest contribution to NOx gases in the urban atmosphere comes from automotive emissions [4-7]. This presents society with the conflict between its dependence on automotive transport and the consequent negative health impacts of polluted air.

Semiconductor photocatalysis has been presented and trialed as a practical solution to the NOx pollution issue since the 1980s [8-10]. TiO_2 has been the most widely applied photocatalyst in construction materials, e.g. in glass and concrete products, and its photocatalytic *activity*, i.e. the rate of normalized NOx concentration decrease, has been exclusively used as an indicator of efficiency [11-17]. The nature of the exposure regimes (of the photocatalyst to light and reactants) is the primary differentiating factor for the various approaches to supporting photocatalysts and has led to a number of innovative and effective strategies for performance improvements [18-20]. However, photocatalytic activity is not, by itself, a useful indicator of the *effectiveness* of the photocatalyst in addressing the issue of air quality. The impact of NOx on health is addressed by the toxicity of its components (and their downstream environmental/photochemical reaction products). In this respect, NO_2 is considerably more toxic than NO (probably by a factor of 10) and so the photocatalytic efficiencies for the oxidation of the individual NOx components is of more relevance.

Photocatalytic NOx oxidation may be considered a step-wise reaction

$$NO \rightarrow HNO_2 \rightarrow NO_2 \rightarrow NO_3^-$$

To be an *effective* photocatalyst, the conversion of the toxic NO_2 to NO_3^- needs to be more efficient than the conversion of NO to NO_2 to ensure that ambient as well as photocatalytically generated NO_2 is removed from the atmosphere. Such a catalyst would demonstrate a high nitrate *selectivity* and could be expected to have a significant positive effect on the resulting air quality. In a recent study by Bloh, *et al* [21], a DeNOx index was presented which showed that several commercial TiO_2 photocatalysts, although demonstrating a high activity, showed a very poor nitrate *selectivity*, with large negative DeNOx indices.

Despite the importance of nitrate selectivity on NOx photocatalysis, the factors which control nitrate selectivity on TiO_2 are still not quantitatively understood, although the principle reaction stages can be readily identified:

- adsorption processes for NO and NO_2 including competition for sites
- energetics governing charge transfer processes following photocatalyst activation
- desorption efficiency of oxidation products

The objective of the present study was to examine the influence of TiO_2 surface chemistry on nitrate selectivity, particularly the role played by water. To ensure maximum exposure of TiO_2 surfaces to reactants, photocatalysts were supported on particulate quartz substrates, a practice which is increasing in real world applications. Nanoparticle TiO_2 hydrosol suspensions were prepared from a low temperature precipitation-peptization process [22-24]. pH control was subsequently used to condition quartz and TiO_2 surface charges, to (i) exploit electrostatic interactions between photocatalyst and substrate, and (ii) vary the ratio of chemi-sorbed (OH) groups to physi-sorbed (H_2O) water on the TiO_2 surfaces, prior to photocatalytic measurements.

2. Materials and Methods

2.1 Raw materials

Quartz sand (SiO_2, 20-50 μm), tetrabutyl orthotitanate (TBOT) ($Ti(OBu)_4$, 97%), HNO_3 (nitric acid, 70 wt.%), absolute ethanol (C_2H_5OH, 99%) and NaOH (sodium hydroxide, 1 M) were purchased from Sigma-Aldrich. Deionized water (18.2 MΩ.cm) was used throughout the preparation process.

2.2 Methods

A low temperature precipitation-peptization process was used to prepare TiO_2 hydrosols using a reaction mixture of TBOT: C_2H_5OH: H_2O: HNO_3 with overall volume ratio 1: 3: 10: 0.08 [25] as follows: TBOT (10 ml) was dissolved in absolute ethanol (15 ml), with stirring for about 30 min at 40 ^oC (Solution A). HNO_3 (8 ml) and absolute alcohol (15 ml) were mixed in deionized water (100 ml), and stirred for 10 min (Solution B). Solution A was then slowly added into solution B with a speed of 1 – 2 drop/s. Finally, the mixture was continually stirred for 48 h, and then aged for 72 h at room temperature.

The TiO_2-quartz composites were prepared as follows: quartz particles were added into TiO_2 hydrosol suspensions (30 ml, 1.68 g TiO_2 equiv./L) of different pH values to give a theoretical mass ratio of TiO_2:quartz (SiO_2) = 0.2 : 0.8. pH was adjusted to values between 1 and 13 using additions of 1 M HNO_3 or 1 M NaOH solutions as required. Suspensions were then stirred for 48 h at room temperature. After that, the suspension solution was centrifuged and washed with water and absolute ethanol (3 water + 1 ethanol) to neutral pH. Subsequently, the precipitates were dried at 105 ^oC for 24 h and/or calcined at 500 ^oC for 3 h. Suitably sized particles were then obtained by sieving out the particles smaller than 20 μm and larger than 50 μm. Samples were marked as TQ-m-n, where m and n represent loading

pH value and temperature, respectively. Pure TiO_2 particles were also obtained by drying TiO_2 hydrosols at 105 ^oC for 24 h.

2.3 Characterization

X-ray diffraction (XRD) patterns were recorded on a PHILIPS P W 3O4O/60X′PertPRO diffractometer in the range 20 to 70 ^{o} 2θ under Cu Kα radiation at a scanning speed of 6 ° min^{-1} and Fourier transform infrared (FT-IR) spectra were obtained using a Perkin-Elmer Spectrum 2 spectrometer. The specific surface area (SSA) was measured on an ASAP 2020 (Micromeritics), using nitrogen adsorption and the morphologies of samples were observed by transmission electron microscopy (TEM, JEM 2000EX). The particle size distribution and surface potential were measured using a Malvern Zetasizer Nano Series analyser (ZS-90). Thermogravimetry and differential thermal analysis (TG-DTA, STA-780) were used to determine the weight loss of samples in the temperature range 25 ^oC to 1000 ^oC utilising a heating rate of 5 ^oC /min in nitrogen atmosphere. Prior to TG-DTA, samples were stored at approximately 40% relative humidity until constant weight. As the surface area of quartz is very low and there is no measured thermal desorption of water from quartz, the data shown are representative of supported TiO_2 only.

2.4 Photocatalytic performance

Photocatalytic performance measurements on prepared samples were carried out in a flow-through reactor (ISO 22197-1: 2007) schematically illustrated in (Figure S1). The supported TiO_2 sample (0.5 g) was uniformly distributed in a rectangular recess (area 2.4 × 10^{-3} m^2) inside the reactor so the NO gas had to flow over the sample surface. The sample was irradiated by an Ultra-Vitalux 300W (Osram, Germany) light source. 1ppm of NO gas in synthetic air, conditioned at a constant 40% relative humidity, measured using a HygroPalm 1 detector (Rotronic) at 25 ^oC, was passed at a volumetric flow rate of 5 × 10^{-5} m^3 s^{-1} through the reactor. The concentrations of NO, NO_2 and NOx were monitored using a Thermo

Scientific Model 42i-HL High Level NO-NO_2-NOx Analyzer (Air Monitors Ltd., United Kingdom). Each sample was measured in the dark until equilibrium concentrations were reached and afterwards, under illumination, until steady state concentrations were observed. The resulting photon flux at the position of the sample was measured to be 3.05×10^{-6} mol s^{-1} m^{-2} using a broadband thermopile detector (Gentec-EO-XLP12-3S-H2-D0). For comparison, the photocatalytic performances of pure TiO_2, Aeroxide® P25 and CristalACTiV™ PC 105 (0.1 g) were measured under identical conditions. The photocatalytic efficiency (ξ) was calculated according to equation (1). The catalyst selectivity for nitrate (S) was calculated according to equation (2).

$$\xi = \frac{(c_d - c_i)VP}{\Phi ART} \qquad (1)$$

$$S = \frac{\xi_{NO_X}}{\xi_{NO}} \qquad (2)$$

where c_d is the concentration in dark, c_i the concentration under illumination, V the volumetric flow rate, p the pressure, A the irradiated sample area, R the gas constant, T the absolute temperature and Φ the photon flux impinging the photocatalyst surface. The photocatalytic efficiency was determined separately for NO, NO_2 and total NOx.

3. Results and Discussion

3.1 Physical and chemical properties

Figure 1 shows an XRD pattern of the prepared TiO_2 particles from which mainly anatase and brookite (< 9 wt % relative to anatase, determined by Rietveld refinement and QXRD [26]) are identified. Lattice fringes of 0.35 nm can be seen in the HRTEM image (Figure 1 inset) which correspond to (101) faces of anatase. Particle size distribution data indicate that the dispersed TiO_2 hydrosols have primary particle sizes in the range 5-10 nm but have agglomerates which reach around 120 nm. Discrete particles and agglomerates in this size

range can also be observed in the TEM image shown (S2) but the elevated temperature and drying conditions during further processing induces further agglomeration and larger clusters as is also indicated by the TEM image. X-ray diffraction line broadening is greater than predicted from the observed particle sizes indicating a relatively low level of crystallinity overall [22].

The level of TiO_2 loading on quartz is dependent on loading pH as is shown in Table 1 (and in Figure S3). TiO_2:SiO_2 mass ratios were determined by QXRD (ICDD cards 71-1169, 78-2486, 84-1286, 75-0589, 27-1402) [26-27] and account was taken of the low level TiO_2 crystallinity by integrating the areas under the relevant diffraction peaks. Because the particles smaller than 20 μm have been screened out, the TiO_2 particles included in subsequent analyses can either be associated with coatings on the quartz or, less likely, as agglomerates greater in size than 20 μm. As expected, samples calcined at 500 ^oC for 3 h show increased levels of crystallinity (sharper XRD peaks; Figure S3) at both loading pH values (pH = 5.14, 13.01).

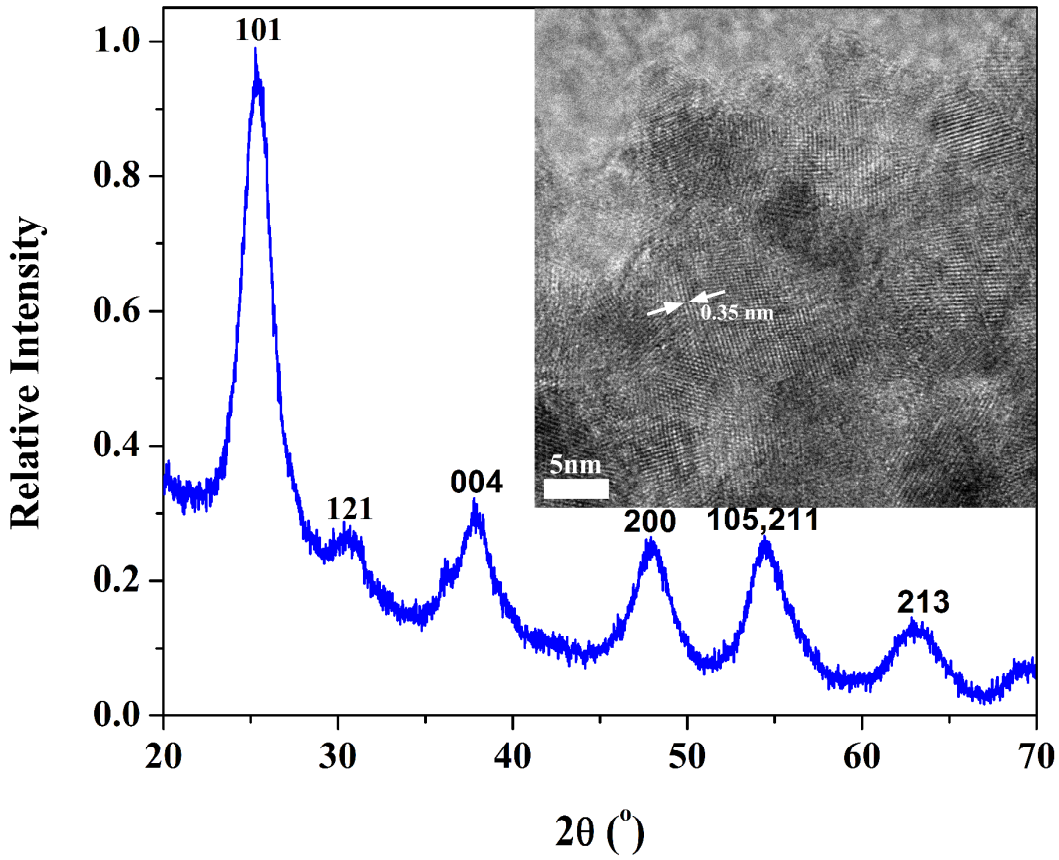

Figure 1. XRD pattern of prepared TiO_2 hydrosols dried at 105 °C with HRTEM image (inset)

The thermogravimetric behavior of the TiO_2-quartz samples is similar in all cases and is rather monotonic. Reports from the literature [28-30] identify the loss of physically adsorbed water (H_2O) between 30 and 120 °C, and of different types of chemically adsorbed water (OH groups) in three clear steps at ca. 300 °C, 460 °C and 600 °C. Although the profile (see Figure S4) does not show any clear discontinuity at 120°C, this temperature is taken to mark the boundary between physi- and chemi-sorbed water for the purposes of discussion.

Table 1 Physical and chemical characteristics of the TiO_2–coated quartz composites.

Sample	TiO_2/ (TiO_2+SiO_2) (Wt %)	SSA_{BET} (m^2/g)	Mass loss % (w/w)		H_2O/ (OH+H_2O)
			H_2O (25 – 120 °C)	OH (120 – 1000 °C)	

TQ-1.67-105	1.8±0.30	8.6	0.086	0.49	0.148
TQ-3.85-105	3.4±0.60	74.9	1.07	2.31	0.317
TQ-5.14-105	5.9±0.75	71.5	1.32	1.23	0.518
TQ-6.03-105	2.7±0.45	73.4	1.19	1.47	0.447
TQ-8.84-105	3.2±0.55	73.1	1.29	1.57	0.450
TQ-13.01-105	3.0±0.50	59.9	1.40	1.51	0.482
TQ-13.01-500	4.8±0.70	22.6	0.25	0.096	0.725
TiO_2-13.01-105	-	321.1	5.84	6.66	0.467
PC105	-	78.9	0.84	1.41	0.375

TiO_2 mass fraction (%) in TQ samples, calculated by QXRD [27]; H_2O – physi-sorbed water; OH- chemi-sorbed water –the ratio normalises these data enabling a comparison between samples

The ratio of physisorbed to total adsorbed water (chemi-+physi-), $H_2O/(OH + H_2O)$, is shown in Table 1 to increase with increasing loading pH up to pH 5, where it gradually stabilises. Also included in Table 1 are the data for TQ-13.01-500 (calcined at 500 ^oC) which shows a significantly increased ratio (mainly signifying a decrease in the fraction of chemi-sorbed water, likely to indicate a higher level of condensation in the Ti-O bonding network than at lower treatment temperatures). Note that the surface bound water quantities are significantly lower at 500 than at 105 ^oC.

The relative TiO_2 loadings indicated in Table 1 can be explained by considering the surface characteristics of the TiO_2 and of its support. The zeta potential (ζ) variation of TiO_2 hydrosols with pH is very similar to that reported elsewhere for TiO_2 [31] but the point of zero charge (PZC) is slightly lower, around pH 5.2 (see Figure S5 and Zhang, *et al* [32]). In the region of this pH, where ζ is ±20 mV (pH 4.5 to 6), TiO_2 is indifferent to either positively or negatively charged surfaces. It also tends to agglomerate because there is insufficient electrostatic repulsion between particles. As pH decreases from the PZC, the increasing positive charge on TiO_2 is increasingly attracted to the negative charge on SiO_2 although the latter reduces to zero at pH ~2.6 (PZC of SiO_2). A pH window therefore exists in which the attractive interaction between TiO_2 and SiO_2 is maximised ($2.6 < pH < 5.2$). Therefore, at the

lower end of this pH range, TiO_2 agglomerates would be expected to electrostatically associate with the quartz surface and this explains the largest level of TiO_2 coating on SiO_2 in the loading pH range 2.6 < pH < 5.2 as indicated by the quantitative XRD results (Table 1).

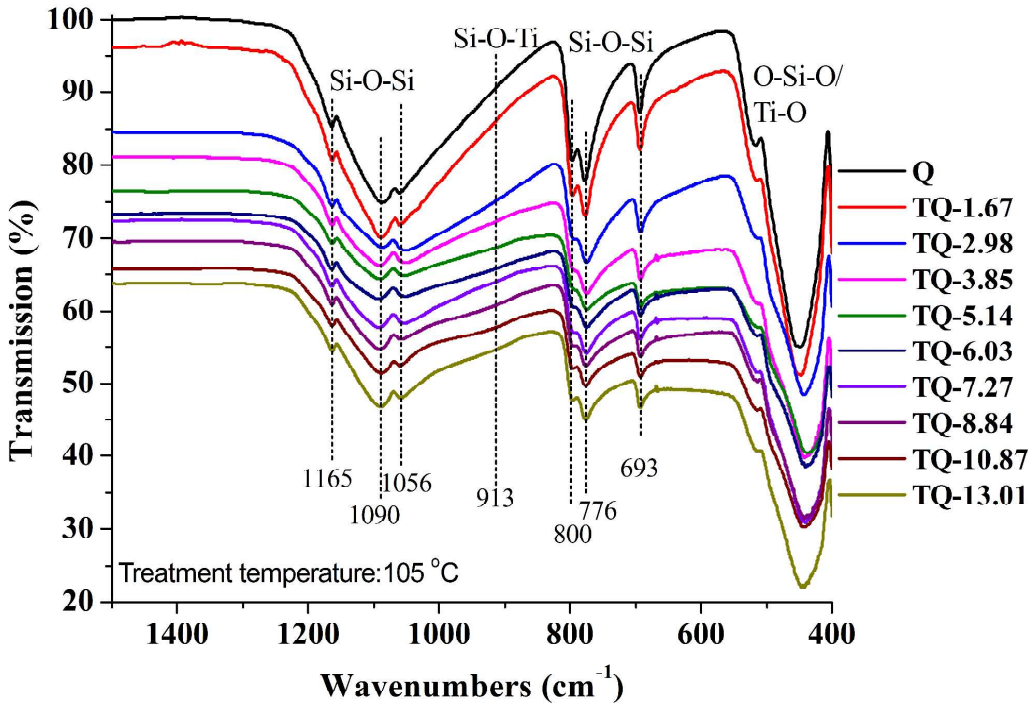

Figure 2. FT-IR spectra of quartz (Q) and TiO_2-quartz (TQ) samples with loading pH values in the range 1.67 -13.01, dried at 105 °C.

The FT-IR spectra for quartz (Q) and TiO_2-quartz (TQ) samples dried at 105 °C for 24 h are shown in Figure 2. The absorption bands at 1165, 1090 and 1056, and between 400 and 800 cm^{-1} are attributed to the vibrations of Si-O bonds [33-35] but other contributions from Ti species may overlap in the 400 and 800 cm^{-1} range (see Figure S6). The weak but broad absorption in the range 900 - 960 cm^{-1}, particularly evident at loading pHs ≥ 8.84, is attributed to Ti-O-Si and is interpreted as representing a chemical linkage between the quartz support and the TiO_2 photocatalyst particles [36]. For these samples, the intensity of absorption around 913 cm^{-1} is therefore indicative of the effectiveness of photocatalyst-support binding.

From a geometrical perspective, the points of contacts between suspended TiO_2 and SiO_2 will be limited to relatively small fractions of the available surface area and this presents an important limiting factor to the number of chemical linkages that can be established under any conditions. Further, the reactivity of the SiO_2 and TiO_2 surfaces is promoted by alkaline hydrolysis, the result of which would be a condensation reaction to form the Ti-O-Si linkage where TiO_2 and SiO_2 have come in contact. At preparation pHs lower than around 9, it is anticipated that SiO_2 and TiO_2 surfaces are insufficiently activated so chemical linking through condensation would be limited, accounting for the absence of absorption around 913 cm^{-1} for samples prepared at pH < 9. Although the conditions of the highest TiO_2 loading correspond to a preparation pH of 5.14, a chemical linkage is unlikely, and is not supported by the FTIR data. Instead, the quartz – TiO_2 connection is believed to be physical, defined by attractive surface charges, consolidated under mild heat treatment.

It is also unlikely that the relatively high amount of TiO_2 particles associated with the loading pH of 5.14 has diluted the intensity of the Ti-O-Si absorption. There is no evident FTIR intensity trend with pH to support this. However, for the sample prepared at the same pH but at higher temperature (500 ^oC) which displays no Ti-O-Si absorption at 913 cm^{-1}, this explanation is reasonable, due to its higher TiO_2:SiO_2 ratio (4.8) (see Figure S6, which also highlights the key wavenumbers for absorption bands relevant to this system).

3.2 Photocatalytic performance

The concentration profiles observed during NOx photocatalysis for all SiO_2-TiO_2 composites were similar to each other (see example in Figure 3) and to those widely reported in the literature for NOx photocatalysis on TiO_2 in general [15]. Three regions can be defined: 1) concentration stabilization without UV light illumination, 2) photocatalytic reaction (light on), 3) concentration stabilization after illumination (light off). NO_2 concentration increases quite rapidly upon sample illumination, and remains almost constant whilst NO concentration

increases slightly, possibly associated with a reduction in access to catalytic sites (possibly by NO_3^-). When the light is switched off, NO_2 production drops to zero.

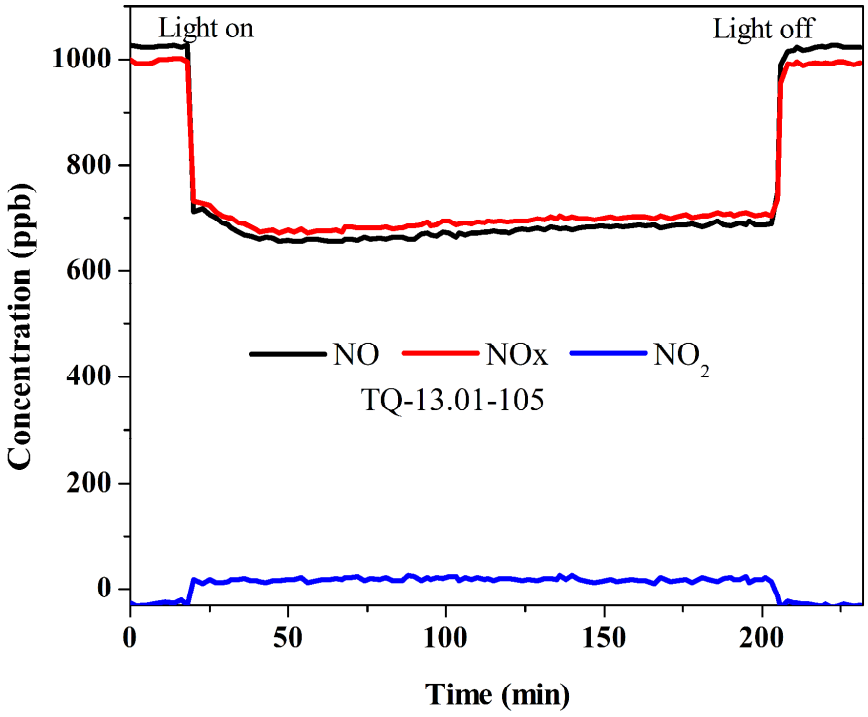

Figure 3. Concentration profiles for NO, NO_2 and NOx ($NO+NO_2$) during the photocatalytic oxidation of NO on TiO_2 supported on quartz (TQ-13.01-105; loading pH value of 13.01)

Figure 4 shows the photonic efficiency (ξ) of NO, NOx removal and NO_2 generation for all samples, calculated according to equation (1). XRD analysis indicated the presence of anatase and brookite polymorphs of TiO_2 but it is reported that brookite has a similar photocatalytic activity for NO oxidation to anatase [21]. Photocatalytic trends observed for these samples are therefore considered to be due to the predominant anatase content. In general, it can be noted that almost all of the composite materials show higher ξ values for NO and NOx conversion than the unsupported commercial TiO_2.

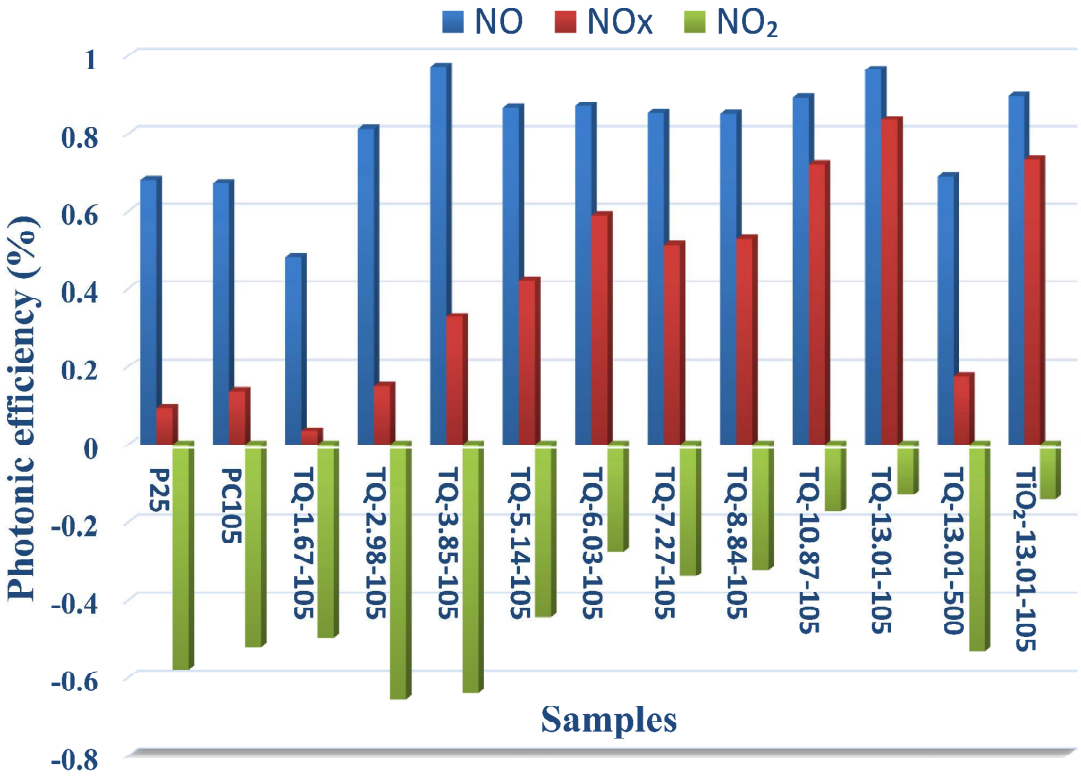

Figure 4. Conversion efficiencies for NO, NO_2 and NOx for various samples

ξ(NO) increased on TiO_2-SiO_2 composites with increasing loading pH in the low pH range but was relatively constant at >80% for pHs above 4.0. In this region, the production rate of NO_2 decreases (decreasing -ξ(NO_2)) which drives a corresponding increase in ξ(NOx) and nitrate selectivity, the latter achieving a maximum at about 86% for pH 13.01 (Figure S7); the nitrate selectivity of the composite calcined at 500 ^{o}C is reduced by around 60% compared with that at 105 ^{o}C (Figure 7 SI). Temperature dependent factors such as degree of TiO_2 crystallinity and defect concentration [38] should be considered as potential explanations but, given the sensitivity to loading pH discussed above, it is tempting to focus on surface composition and surface structure as the dominant effects, i.e. distribution of hydroxylated surface species, which influence adsorption/desorption characteristics [39-40].

In principle, the photocatalysis process can be divided into three mechanistic steps: (1) the adsorption of target molecules, (2) degradation of adsorbed molecules under light illumination, and (3) desorption of degraded substances. Adsorption is a competitive process and NO and NO_2 molecules compete for adsorption sites, which include sites provided by chemisorbed water [40-42]. Molecular (physisorbed) water also participates in the photocatalytic process [43-44], so the distribution of physi- and chemi-sorbed water is likely to be an important controlling variable in defining photocatalytic efficiency.

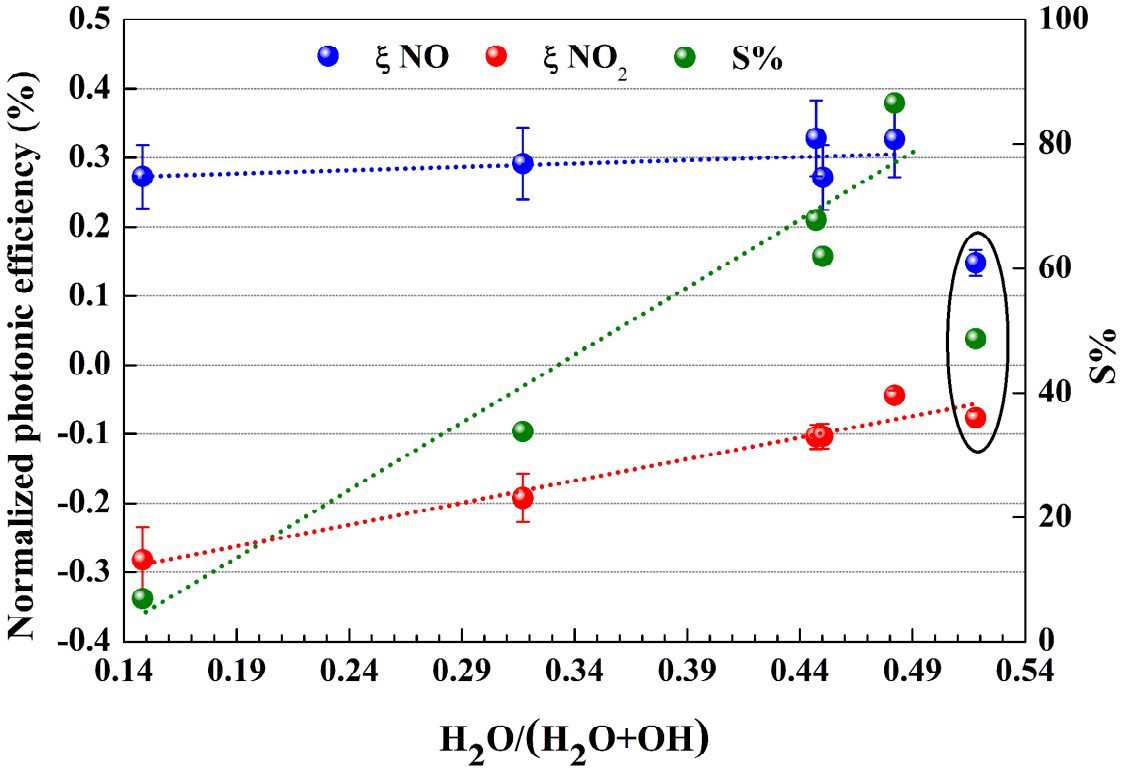

Figure 5. Relationship between photocatalytic performance and physi-/(chemi + physi-) sorbed water ratio (photonic efficiencies were normalized by TiO_2 loading (wt. %)); loading pH is indicated for each composite in Table 1.

The relationships between *normalized* photocatalytic performance, with respect to TiO_2 loading, and the distribution of physi- and chemi-sorbed water are shown in Figure 5. The low ξ (NO) and ξ (NOx) values of TQ-1.67-105 shown in Figure 4 is therefore attributable to

the low TiO_2 loading on this composite as its normalized ξ(NO) value is similar to that measured for the other composites (Figure 5). Indeed, mass normalized ξ(NO) is almost insensitive to the $H_2O/(OH+H_2O)$ ratio up to a value of 0.48 (almost half the mass fraction range). This suggests that in this range, (i) NO adsorption is not limited by the availability of adsorption sites (e.g. chemisorbed water), and (ii) NO oxidation is not *directly* dependent on physisorbed water content.

Photocatalytic mechanisms. NO_{ads} can be oxidised on the illuminated TiO_2 following several well-established photocatalytic pathways [38, 41, 45-46], (see equations (3)-(8)). In these, adsorbed water plays important but different *indirect* roles:

(i) In reaction with photogenerated charges from (3), it produces $^{\bullet}OH$ (4), which oxidises NO_{ads} in (6). H^+, also produced in (4), participates in oxidising reactions (7) and (8) with $O_2^{\bullet-}{}_{ads}$, produced from (5).

$$TiO_2 + h\nu \rightarrow TiO_2\,(h^+ + e^-) \quad (3)$$

$$TiO_2(h^+) + H_2O_{ads} \rightarrow TiO_2 + {}^{\bullet}OH_{ads} + H^+ \quad (4)$$

$$TiO_2(e^-) + O_{2ads} \rightarrow TiO_2 + O_2^{\bullet-}{}_{ads} \quad (5)$$

$$NO_{ads} \xrightarrow{{}^{\bullet}OH_{ads}} HNO_{2ads} \xrightarrow{{}^{\bullet}OH_{ads}} NO_{2ads} + H_2O \quad (6)$$

$$NO_{ads} \xrightarrow[H^+]{O_2^{\bullet-}{}_{ads}} \begin{cases} NO_{2ads} + {}^{\bullet}OH & (7) \\ HNO_{3ads} & (8) \end{cases}$$

(ii) NO may also be oxidised by terminal oxygen species, $TiO_2(O_s^{\bullet})$, formed upon trapping of the holes by bridging surface oxygen ((9), (10)).

$$TiO_2(h^+) + TiO_2(O_s) \rightarrow TiO_2(O_s^{\bullet}) \quad (9)$$

$$NO_{ads} \xrightarrow[H_2O]{TiO_2(O_s^{\bullet})} TiO_2 + NO_{2ads} + 2H^+ \quad (10)$$

$$NO_{ads} \xrightarrow{TiO_2(O_s^{\bullet})} NO_{2ads} + TiO_2\,(V) \xrightarrow{H_2O} TiO_2 + 2H^+ \quad (11)$$

However, the insensitivity of ξ(NO) to the $H_2O/(OH+H_2O)$ ratio (Figure 5) is in conflict with reaction (10) which is better represented by the equivalent two-stage process shown in

reaction (11). In the overall reaction mechanism, H_2O is only *indirectly* involved in the NO oxidation process, i.e. in neutralising the resulting oxygen vacancy (V), as indicated in Figure 5. Further possibilities for NO oxidation are evident from reactions (7) and (8), each involving the superoxide ion radical, $O_2^{\bullet-}{}_{ads}$ generated from processes (3) and (5). Examination of Figure 3 indicates significantly greater concentration changes arising for NO (~-300 ppb) than for NO_2 (~+30 ppb) upon illumination. Although the concentrations indicated are steady state gas phase concentrations, this difference is typical for all catalysts studied and suggests that NO oxidation is not exclusively to NO_2 and that reaction (8) is more important than was previously thought.

In contrast, Figure 5 shows that NO_2 oxidation, i.e. $-\xi(NO_2)$, is positively correlated with the $H_2O/(OH+H_2O)$ ratio, indicating its *direct* dependence on physisorbed molecular water. Photocatalysed NO_2 oxidation reactions (12) and (13) have been previously proposed [41] but only (13) shows a direct dependency on physisorbed water content. The $\xi(NO_2)$- physisorbed water concentration correlation therefore supports the photo-induced defect mechanism for NO_2 oxidation on TiO_2.

$$NO_{2ads} + {}^{\bullet}OH_{ads} \rightarrow HNO_{3ads} \qquad (12)$$

$$NO_{2ads} \xrightarrow[H_2O]{TiO_2(O_s^{\bullet})} TiO_2 + NO_3^-{}_{ads} + 2H^+ \qquad (13)$$

In addition, the presence of physisorbed water offers further, non-photocatalytic oxidation mechanisms with the overall reaction shown in (14) [15, 47]. These are usually ignored when discussing the photocatalytic conversion of NO_x to NO_3^-, as are the solubilities of the resulting species, which are likely to play an important role in removing oxidation products from catalytic sites.

$$3NO_2 + H_2O \rightarrow NO + 2HNO_3 \qquad (14)$$

Nitrate selectivity. The effectiveness of a photocatalyst in atmospheric de-NOx processes may be measured by its nitrate selectivity; the extent to which the direct oxidation of NO to NO_3^- is favoured over the production of the more toxic NO_2 intermediate [21]. Figure 5 indicates a proportional nitrate selectivity increase with physisorbed water concentration across the range $0.15 < H_2O/(OH+H_2O) < 0.48$, which is related to the equivalent trend in $\xi(NO_2)$. This observation is important because it suggests that the nitrate selectivity of TiO_2 is not only influenced by molecular water but also by the level of photo-induced structural defects (i.e. oxide ion vacancies) in the photocatalyst, as indicated in reaction (13). This relationship between defect concentration and nitrate selectivity in TiO_2 has been suggested before [38] and these results may provide some support for this, although in the present case, the linear dependency of selectivity with physisorbed water content suggests that defect concentration is not a limiting factor.

To establish the relative importance, quantitatively, of photocatalytic (e.g. 13) and non-photocatalytic (14) processes for the conversion of NO_2, a sample (TQ-13.01-105) was exposed to NO_2 in the reactor and concentrations of NO and NO_2 were monitored over time through a program of dark and illuminated stages (Figure 6). NO_2 initially at approximately 230 ppb, stabilized in the by-pass circuit, was introduced to the dark reactor and immediately, a drop in concentration was observed. This could be due to chemical conversion through non-photocatalytic processes but the observation that concentration starts to rise throughout the remaining dark period suggests that the adsorbed NO_2 is being displaced by competitive adsorption through the introduction of water (NO_2 supplied with 40% relative humidity). This interpretation is supported by the relatively small NO concentration change upon illumination (see later). This rise in NO_2 concentration continues until the initial NO_2 concentration is re-established indicating only limited chemical conversion during the dark phase.

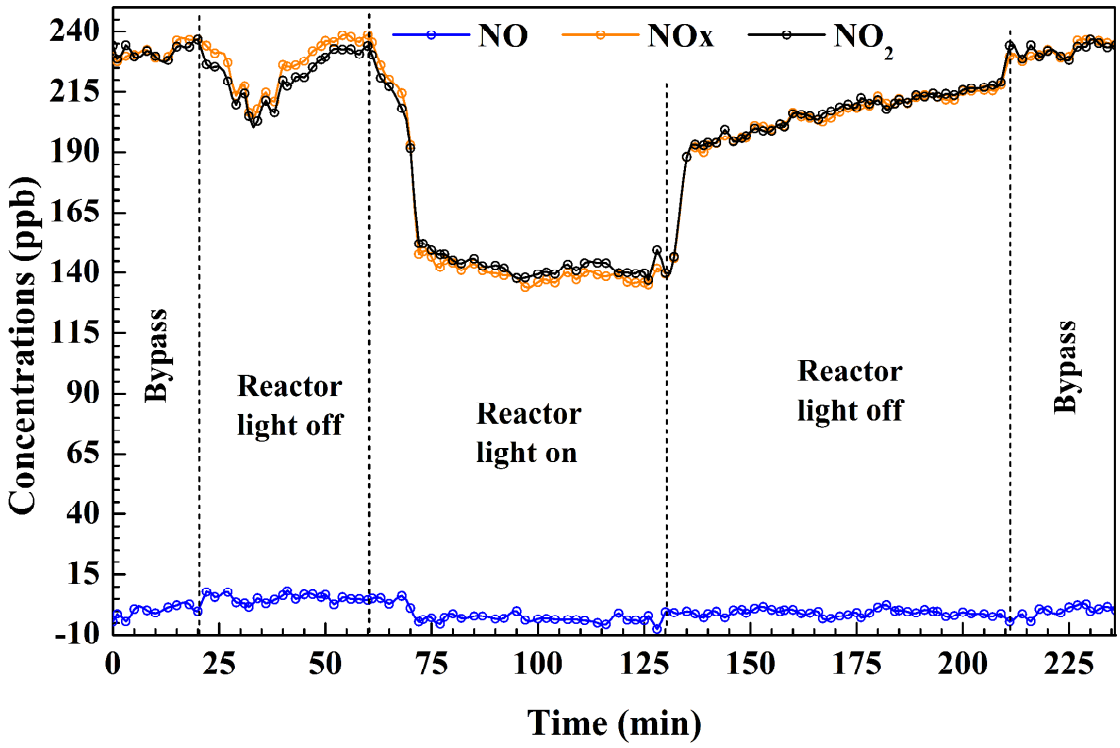

Figure 6. Concentration profiles for NO, NO_2 and NOx ($NO+NO_2$) during flowing of NO_2 over TiO_2 supported on quartz (TQ-13.01-105; loading pH value of 13.01) through a programme of dark and illuminated stages.

Upon illumination, the NO_2 concentration drops gradually and then, after a short time delay (10 minutes), more rapidly. It is proposed that two effects are responsible:

- the photocatalytic processes summarized above facilitating
  - the oxidation of NO, formed from NO_2 adsorbed on TiO_2 during the dark phase (reaction (14))
  - the oxidation of NO_2
- the restructuring of TiO_2 surface sites (the well-known superhydrophylicity effect) increases the concentration of surface hydroxide groups (chemisorbed water) and the availability of binding sites for NO but decreases those for NO_2, causing gas-phase NO_2 concentration to increase.

Competition between these effects may account for the delay in the concentration reduction observed but this reduction under illumination highlights the importance of photocatalytic mechanisms over dark chemical conversion. Note that upon illumination, the reduction in NO concentration due to photocatalysis, is an indicator of the generation of NO in the dark phase (reaction (14)). This small effect confirms that the photocatalytic contribution to NO_2 oxidation on TiO_2 is the dominant oxidation mechanism.

Opportunities for implementation. Identification of physisorbed water content as an important variable in defining nitrate selectivity of TiO_2 photocatalysts presents an important opportunity for addressing NOx-related air quality issues. Coupled with the availability of oxide ion vacancies [38, 47-48] on TiO_2 surfaces (see equation 13), control of adsorbed water distribution can potentially allow for the engineering of high nitrate selectivity TiO_2 photocatalysts. Photocatalysts with the highest physisorbed water content appear to have the highest nitrate selectivity but control of humidity, whilst not only impractical in a real application, is unlikely to provide a solution. At increased relative humidity, condensed liquid water on photocatalyst surfaces is expected to limit access to surface catalytic sites. Instead, pH control during surface conditioning has shown to be a useful method for generating optimum water distribution on TiO_2 rather than the control of humidity.

Figure 7 shows how these TiO_2 materials perform in relation to the DeNOx index, defined by Bloh et al [21], which provides a numerical indicator of photocatalyst effectiveness. Positive DeNOx values identify photocatalyst performances which can be expected to reduce atmospheric NO_2 and improve air quality. It is shown that samples conditioned at pH 6 and higher are environmentally applicable. It can be noted that the sample conditioned at pH 13 has the most positive DeNOx index. This photocatalyst is chemically bonded to its support but the effect of bonding will be discussed elsewhere.

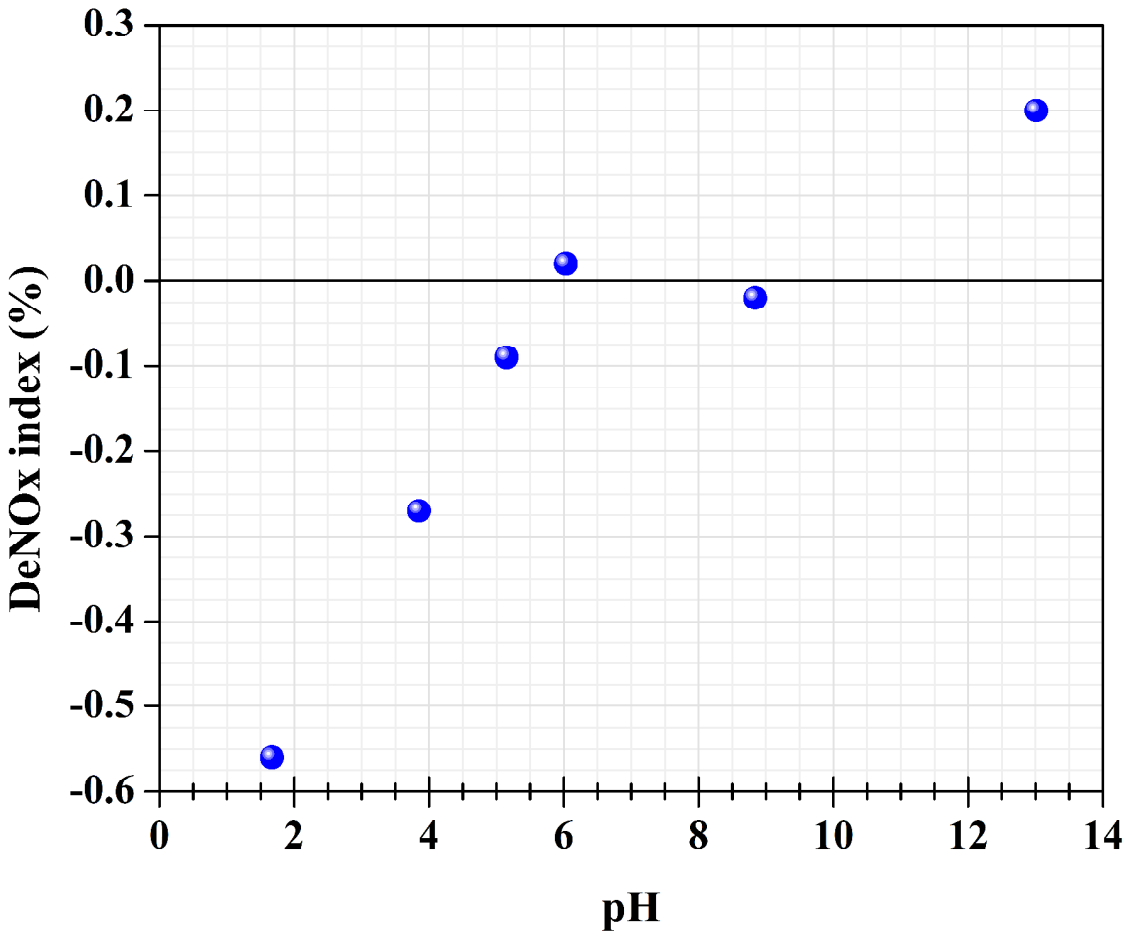

Figure 7. The DeNOx index for the TiO_2 supported on quartz samples in dependence of their pH conditioning.

4. Conclusions

A low temperature precipitation-peptization process was used to produce nano-dimensional TiO_2 which was conditioned under different pH in mixtures with particulate quartz. TiO_2-SiO_2 composites were produced with different levels of TiO_2-SiO_2 binding and with controlled TiO_2 surfaces having a range of adsorbed water compositions (different physi-sorbed/chemi-sorbed water ratios).

Almost all of the supported TiO_2 (on quartz) samples show higher photocatalytic conversion efficiencies for NO and NOx than the unsupported commercial TiO_2. This

confirms earlier findings [49]. The role of water in defining photonic efficiency is highlighted, particularly the distribution of chemisorbed and physisorbed water on the TiO_2 surface. The insensitivity of ξ(NO) to the mass fraction of physisorbed water in the range 0.15 to 0.48 (Figure 5) indicates that molecular water only has an indirect role in NO oxidation, i.e. in providing $^{\bullet}$OH. In contrast, the strong $\xi(NO_2)$ correlation indicates *direct involvement with water*, which identifies a photo-induced defect mechanism for NO_2 photocatalytic oxidation; a dark oxidation pathway for NO_2 conversion was shown to be active but quantitatively much less important than the photocatalytic route. This important observation provides a mechanistic differentiation for the photocatalytic NO and NO_2 oxidation reactions offering an interpretation for the different nitrate selectivities observed for TiO_2. Indeed, the mechanism identified here suggests that greater focus may be given to previous observed correlations between selectivity and defect concentrations, particularly in the context of adsorbed water distribution. A correlation between the DeNOx index of Bloh et al [21] and photocatalyst conditioning pH presents a practical approach to conditioning surface water distributions on TiO_2 and together with methods for manipulation of surface defect concentrations, may offer a focus towards more effective use of TiO_2 photocatalysis in maximising DeNOx strategies for urban atmospheres.

Notes

The authors declare no competing financial interest.

Acknowledgements

The authors gratefully acknowledge funding from the UK Engineering and Physical Sciences Research Council (Grant Ref: EP/M003299/1) and the Natural Science Foundation of China (No. 51461135005) International Joint Research Project (EPSRC-NSFC).

Supporting Information

Supporting Information is available free of charge on the ACS Publications website at http://pubs.acs.org.

Schematic of the experimental configuration, particle size distribution data, HRTEM image of the TiO_2 particles, XRD patterns details, typical TGA profile, zeta potential data, FT-IR spectra data, and nitrate selectivity data.

5. References

(1) Morrow, P. E. An Evaluation of Recent NOx Toxicity Data and an Attempt to Derive an Ambient Air Standard for NOx by Established Toxicological Procedures. *Environ. Res.* 1975, *10*, 92-112.

(2) Singh, H. B.; Salas, L. J.; Viezee, W. Global Distribution of Peroxyacetyl Nitrate. *Nature* 1986, *321*, 588-591.

(3) Al-Alawi, S. M.; Abdul-Wahab, S. A.; Bakheit, C. S. Combining Principal Component Regression and Artificial Neural Networks for More Accurate Predictions of Ground-Level Ozone. *Environ. Modell. Softw* 2008, *23*, 396-403.

(4) Wik, C.; Niemi, S. Low Emission Engine Technologies for Future Tier 3 Legislations - Options and Case Studies. *J. Shipp. Trd.* 2016, *1*, 3.

(5) EU Emission Standards. https://www.dieselnet.com/standards/eu/ld.php#stds (accessed Jan 11, 2017).

(6) Transportation, G. Ge Transportation Delivers First Epa Tier 4 Emissions-Compliant Marine Diesel Engines Featuring Breakthrough Technology. http://www.getransportation.com/news/ge-transportation-delivers-first-epa-tier-4-emissions-compliant-marine-diesel-engines-featuring (accessed Feb 01, 2017).

(7) US-EPA Emission Standards Reference Guide. https://www.epa.gov/emission-standards-reference-guide/all-epa-emission-standards (accessed Dec 21, 2016).

(8) Hanus, M. J.; Harris, A. T. Nanotechnology Innovations for the Construction Industry. *Prog. Mater. Sci.* 2013, *58*, 1056-1102.

(9) Mills, A.; Elouali, S. The Nitric Oxide ISO Photocatalytic Reactor System: Measurement of NOx Removal Activity and Capacity. *J. Photoch. Photobio. A* 2015, *305*, 29-36.

(10) Cassar, L. Photocatalysis of Cementitious Materials: Clean Buildings and Clean Air. *Mrs. Bull.* 2004, *29*, 328-331.

(11) Seo, D.; Yun, T. S. NOx Removal Rate of Photocatalytic Cementitious Materials with TiO_2 in Wet Condition. *Build. Environ.* 2017, *112*, 233-240.

(12) Mendoza, C.; Valle, A.; Castellote, M.; Bahamonde, A.; Faraldos, M. TiO_2 and TiO_2–SiO_2 Coated Cement: Comparison of Mechanic and Photocatalytic Properties. *Appl. Catal. B: Environ*. 2015, *178*, 155-164.

(13) Krou, N. J.; Batonneau-Gener, I.; Belin, T.; Mignard, S.; Horgnies, M.; Dubois-Brugger, I. Mechanisms of NOx Entrapment into Hydrated Cement Paste Containing Activated Carbon — Influences of the Temperature and Carbonation. *Cement Concrete Res.* 2013, *53*, 51-58.

(14) Folli, A.; Pade, C.; Hansen, T. B.; De Marco, T.; Macphee, D. E. TiO_2 Photocatalysis in Cementitious Systems: Insights into Self-Cleaning and Depollution Chemistry. *Cement Concrete Res.* 2012, *42*, 539-548.

(15) Ângelo, J.; Andrade, L.; Madeira, L. M.; Mendes, A. An Overview of Photocatalysis Phenomena Applied to NOx Abatement. *J. Environ. Manage.* 2013, *129*, 522-539.

(16) Ballari, M.; Hunger, M.; Hüsken, G.; Brouwers, H. J. H. NOx Photocatalytic Degradation Employing Concrete Pavement Containing Titanium Dioxide. *Appl. Catal. B: Environ.* 2010, *95*, 245-254.

(17) Kamaruddin, S.; Stephan, D. Quartz–Titania Composites for the Photocatalytical Modification of Construction Materials. *Cement Concrete Comp.* 2013, *36*, 109-115.

(18) Guo, M. Z.; Poon, C. S. Photocatalytic NO Removal of Concrete Surface Layers Intermixed with TiO_2. *Build. Environ.* 2013, *70*, 102-109.

(19) Chen, J.; Poon, C. S. Photocatalytic Activity of Titanium Dioxide Modified Concrete Materials – Influence of Utilizing Recycled Glass Cullets as Aggregates. *J. Environ. Manage.* 2009, *90*, 3436-3442.

(20) Wang, F. Z.; Yang, L.; Wang, H.; Yu, H. G. Facile Preparation of Photocatalytic Exposed Aggregate Concrete with Highly Efficient and Stable Catalytic Performance. *Chem. Eng. J.* 2015, *264*, 577-586.

(21) Bloh, J. Z.; Folli, A.; Macphee, D. E. Photocatalytic NOx Abatement: Why the Selectivity Matters. *RSC Adv.* 2014, *4*, 45726-45734.

(22) Bansal, V.; Li, Y.; Qin, Z.; Guo, H.; Yang, H.; Zhang, G.; Ji, S.; Zeng, T. Low-Temperature Synthesis of Anatase TiO_2 Nanoparticles with Tunable Surface Charges for Enhancing Photocatalytic Activity. *PLoS ONE* 2014, *9*, e114638.

(23) Burunkaya, E.; Akarsu, M.; Erdem Çamurlu, H.; Kesmez, Ö.; Yeşil, Z.; Asiltürk, M.; Arpaç, E. Production of Stable Hydrosols of Crystalline TiO_2 Nanoparticles Synthesized at Relatively Low Temperatures in Diverse Media. *Appl. Surf. Sci.* 2013, *265*, 317-323.

(24) Liu, T. X.; Li, F. B.; Li, X. Z. TiO_2 Hydrosols with High Activity for Photocatalytic Degradation of Formaldehyde in a Gaseous Phase. *J. Hazard. Mater.* 2008, *152*, 347-355.

(25) Bischoff, B. L.; Anderson, M. A. Peptization Process in the Sol-Gel Preparation of Porous Anatase (TiO_2). *Chem. Mater.* 1995, *7*, 1772-1778.

(26) Chung, F. H. Quantitative Interpretation of X-Ray Diffraction Patterns of Mixtures. I. Matrix-Flushing Method for Quantitative Multicomponent Analysis. *J. Appl. Crystallogr.* 1974, *7*, 519-525.

(27) Lebedev, V. A.; Kozlov, D. A.; Kolesnik, I. V.; Poluboyarinov, A. S.; Becerikli, A. E.; Grünert, W.; Garshev, A. V. The Amorphous Phase in Titania and Its Influence on Photocatalytic Properties. *Appl. Catal. B: Environ.* 2016, *195*, 39-47.

(28) Mueller, R.; Kammler, H. K.; Wegner, K.; Pratsinis, S. E. OH Surface Density of SiO_2 and TiO_2 by Thermogravimetric Analysis. *Langmuir.* 2003, *19*, 160-165.

(29) Di Paola, A.; Bellardita, M.; Palmisano, L.; Barbieriková, Z.; Brezová, V. Influence of Crystallinity and OH Surface Density on the Photocatalytic Activity of TiO_2 Powders. *J. Photoch. Photobio. A* 2014, *273*, 59-67.

(30) Liu, P.; Duan, W.; Liang, W.; Li, X. Thermokinetic Studies of the Groups on TiO_2 Surface. *Surf. Interface. Anal.* 2009, *41*, 394-398.

(31) Folli, A.; Pochard, I.; Nonat, A.; Jakobsen, U. H.; Shepherd, A. M.; Macphee, D. E. Engineering Photocatalytic Cements: Understanding TiO_2 Surface Chemistry to Control and Modulate Photocatalytic Performances. *J. Am. Ceram. Soc.* 2010, *93*, 3360-3369.

(32) Zhang, M.; Shi, L.; yuan, S.; Zhao, Y.; Fang, J. Synthesis and Photocatalytic Properties of Highly Stable and Neutral TiO_2/SiO_2 Hydrosol. *J. Colloid Interf. Sci* 2009, *330*, 113-118.

(33) Tokarský, J.; Matějka, V.; Neuwirthová, L.; Vontorová, J.; Mamulová Kutláková, K.; Kukutschová, J.; Čapková, P. A Low-Cost Photoactive Composite Quartz Sand/TiO_2. *Chem. Eng. J.* 2013, *222*, 488-497.

(34) Wu, L.; Zhou, Y.; Nie, W.; Song, L.; Chen, P. Synthesis of Highly Monodispersed Teardrop-Shaped Core–Shell SiO_2/TiO_2 Nanoparticles and Their Photocatalytic Activities. *Appl. Surf. Sci.* 2015, *351*, 320-326.

(35) Fujishima, M.; Takatori, H.; Tada, H. Interfacial Chemical Bonding Effect on the Photocatalytic Activity of TiO_2–SiO_2 Nanocoupling Systems. *J. Colloid Interf. Sci* 2011, *361*, 628-631.

(36) Yuan, L.; Han, C.; Pagliaro, M.; Xu, Y. J. Origin of Enhancing the Photocatalytic Performance of TiO_2 for Artificial Photoreduction of CO_2 through a SiO_2 Coating Strategy. *J. Phys.Chem. C* 2016, *120*, 265-273.

(37) Tokarský, J.; Čapková, P. Structure Compatibility of TiO_2 and SiO_2 Surfaces. *Appl. Surf. Sci.* 2013, *284*, 155-164.

(38) Ma, J.; Wu, H.; Liu, Y.; He, H. Photocatalytic Removal of NOx Over Visible Light Responsive Oxygen-Deficient TiO_2. *J. Phys.Chem. C* 2014, *118*, 7434-7441.

(39) Fujishima, A.; Zhang, X.; Tryk, D. A. TiO_2 Photocatalysis and Related Surface Phenomena. *Surf. Sci. Rep.* 2008, *63*, 515-582.

(40) Lasek, J.; Yu, Y. H.; Wu, J. C. S. Removal of NOx by Photocatalytic Processes. *J. Photoch. Photobio. C* 2013, *14*, 29-52.

(41) Dillert, R.; Engel, A.; Große, J.; Lindner, P.; Bahnemann, D. W. Light Intensity Dependence of the Kinetics of the Photocatalytic Oxidation of Nitrogen(II) Oxide at the Surface of TiO_2. *Phys. Chem. Chem. Phys.* 2013, *15*, 20876.

(42) Dillert, R.; Stötzner, J.; Engel, A.; Bahnemann, D. W. Influence of Inlet Concentration and Light Intensity on the Photocatalytic Oxidation of Nitrogen(II) Oxide at the Surface of Aeroxide® TiO_2 P25. *J. Hazard. Mater.* 2012, *211-212*, 240-246.

(43) Yi, J.; Bahrini, C.; Schoemaecker, C.; Fittschen, C.; Choi, W. Photocatalytic Decomposition of H_2O_2 on Different TiO_2 Surfaces Along with the Concurrent Generation of HO_2 Radicals Monitored Using Cavity Ring Down Spectroscopy. *J. Phys.Chem. C* 2012, *116*, 10090-10097.

(44) Folli, A.; Campbell, S. B.; Anderson, J. A.; Macphee, D. E. Role of TiO_2 Surface Hydration on NO Oxidation Photo-Activity. *J. Photoch. Photobio. A* 2011, *220*, 85-93.

(45) Freitag, J.; Domínguez, A.; Niehaus, T. A.; Hülsewig, A.; Dillert, R.; Frauenheim, T.; Bahnemann, D. W. Nitrogen(II) Oxide Charge Transfer Complexes on TiO_2: A New Source for Visible-Light Activity. *J. Phys.Chem. C* 2015, *119*, 4488-4501.

(46) Ohko, Y.; Nakamura, Y.; Negishi, N.; Matsuzawa, S.; Takeuchi, K. Photocatalytic Oxidation of Nitrogen Monoxide Using TiO_2 Thin Films under Continuous UV Light Illumination. *J. Photoch. Photobio. A* 2009, *205*, 28-33.

(47) Rubasinghege, G.; Grassian, V. H. Role(s) of Adsorbed Water in the Surface Chemistry of Environmental Interfaces. *Chem. Commun.* 2013, *49*, 3071-3094.

(48) Rodriguez, J. A.; Jirsak, T.; Liu, G.; Hrbek, J.; Dvorak, J.; Maiti, A. Chemistry of NO_2 on Oxide Surfaces: Formation of NO_3 on TiO_2 (110) and $NO_2 \leftrightarrow$O Vacancy Interactions. *J. Am. Chem. Soc.* 2001, *123*, 9597-9605.

(49) Todorova, N.; Giannakopoulou, T.; Karapati, S.; Petridis, D.; Vaimakis, T.; Trapalis, C. Composite TiO_2/Clays Materials for Photocatalytic NOx Oxidation. *Appl. Surf. Sci.* 2014, *319*, 113-120.

Table of Contents